Oxygen and nitrogen interstitial ordering in hcp Ti, Zr, and Hf: An *ab initio* study

A. V. Ruban, V. I. Baykov, and B. Johansson
Applied Material Physics, Department of Materials Science and Engineering, Royal Institute of Technology, SE-100 44 Stockholm, Sweden

V. V. Dmitriev and M. S. Blanter
Moscow State University of Instrumental Engineering and Information Science, Stromynka 20, Moscow 107996, Russia
(Received 13 April 2010; revised manuscript received 30 July 2010; published 14 October 2010)

We investigate the ordering of oxygen and nitrogen interstitials in hcp Zr, Hf, and Ti using the corresponding oxygen-oxygen and nitrogen-nitrogen interactions obtained in the state-of-the-art first-principles calculations. Two main contributions, chemical and strain induced, to the interstitial-interstitial interactions are obtained by different techniques. We find that there is the strong repulsion between interstitial atoms at the nearest- and next-nearest-neighbor coordination shells, which is solely determined by the chemical interaction determined on a fixed ideal lattice, while both contributions are important for more distant coordination shells. The Monte Carlo simulations reveal the existence of three stoichiometric compositions, $MeI_{1/6}$, $MeI_{1/3}$, and $MeI_{1/2}$, for the ground-state structures of interstitials, having different ordering types. Our results for the structures of oxygen interstitials are in good agreement with existing experimental data for the Ti and Hf alloys. In the case of Zr-O interstitial alloys, we correctly predict the general type of ordering, although the detailed structure is at variance the experimental observations. The ordering transition temperatures in some cases are overestimated by a factor of 2. We also predict the ordering type of nitrogen interstitials in hcp Ti, Zr, and Hf, which are similar to those in the case of oxygen interstitials.

DOI: 10.1103/PhysRevB.82.134110 PACS number(s): 61.66.Dk, 61.50.Ah

I. INTRODUCTION

Interstitial solid solutions are formed when atoms of an element having relatively small size, such as hydrogen, oxygen, nitrogen, boron, or similar, occupy interstitial lattice positions between atoms of a host metal. One of the most interesting and experimentally well-studied interstitial solid solutions is an oxygen alloy in hcp Ti, Zr, and Hf. These metals and their alloys have a wide range of technological applications due to their outstanding properties such as high corrosion resistance even in aggressive environment, mechanical strength, biocompatibility, and relatively high melting point. Zirconium is widely used in the nuclear energetics as cladding for nuclear fuel rods due to its low absorption cross section. The high strength-to-weight ratio of titanium alloys makes them indispensable for aerospace and navy applications. In all these cases, oxygen interstitials play important role in the structural stability and other properties of the group-IV materials.

The solubility of oxygen in these metals is large: namely, up to 33, 29, and 20 at. % of oxygen can be dissolved in the octahedral interstitial sites (see Fig. 1) of the hcp Ti, Zr, and Hf, respectively, at room temperature.[1] The latter is a consequence of the relatively large size of the octahedral sites in the hcp lattice, so that when oxygen atoms are dissolved in these metals, they produce relatively small lattice distortions. This is clearly reflected in the moderate rate of the concentration lattice expansion determined as $1/a(da/dx)$, where a is the lattice constant and x is the concentration of interstitial atoms in the interstitial sites, which is of an order of 0.02–0.17, while, for instance, in the case of such bcc metals as V, Nb, and Ta it varies between 0.47 and 0.69.[2] In the latter case, it results in quite restricted solubility of oxygen and displasive transformation of the host lattice due to the oxygen ordering.[3]

Ordered structures of oxygen interstitials in hcp Ti were studied in the x-ray diffraction experiments by Holmberg,[4] who established the low-temperature structure of $TiO_{0.33}$ alloy (α''-Ti_3O). Later, the hcp Ti-O solid solutions have been investigated by different authors,[1,5–8] using x-ray, electron, and neutron-diffraction methods as well as by calorimetry, and the consensus at the moment is that oxygen atoms occupy up to 50% of the octahedral sites forming at this composition the so-called α'-Ti_2O phase below 800 K. Another ordered phase, the so-called α'' phase, is formed at lower temperatures and low oxygen content.[1] Let us note, however, that the α' phase combines two different structures for different ranges of oxygen compositions, one for $TiO_{x<1/6}$ and the other for $TiO_{1/6<x<1/3}$.

The ordering of oxygen interstitials in hcp Zr is quite different: if oxygen atoms avoid each other in the nearest-neighbor (0001) planes of the octahedral interstitial positions in Ti, they occupy every layer in Zr. Although the solubility of oxygen in Zr is slightly less than in Ti, about 29 at. % at room temperature, the ordering of oxygen interstitials seems to be less clear and more complex including the formation of long period superstructures (LPSs).[1,8–12] Oxygen ordering in hcp Hf is again different from that in Zr, however, it is similar to that in Ti in one respect: oxygen atoms occupy the octahedral sites in every second (0001) layer.[1,13] As in the case of Ti-O interstitial alloys, one can distinguish two different types of the oxygen superstructures: one $TiO_{x<1/6}$ compositions and the other one for $TiO_{1/6<x<0.25}$ alloys.

In contrast to the oxygen interstitial alloys, the information about nitrogen interstitial alloys in hcp Ti, Zr, and Hf is very restricted and mostly concerns the solubility of nitrogen. For instance, nitrogen has quite restricted solubility in Ti, which strongly depends on temperature and is about 17 at. % at 1170 K.[14] The solubilities of nitrogen in Zr and Hf

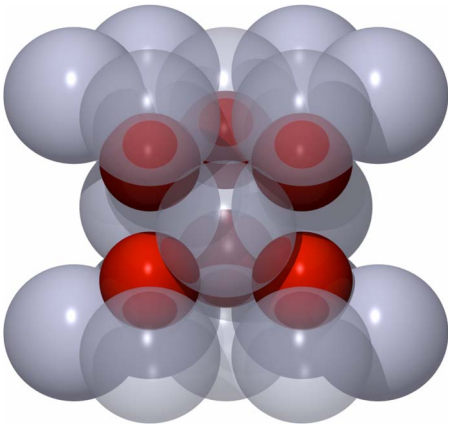

FIG. 1. (Color online) Octahedral sites (small spheres) in hcp structure (large light spheres).

are about 20 and 30 at. %, respectively, at 800 K.[15,16] There is no information about nitrogen ordering in the interstitial positions.

In this paper we investigate the ordering of oxygen and nitrogen interstitials in the hcp Ti, Zr, and Hf on the basis of first-principles calculations of the interstitial-interstitial interactions and subsequent statistical thermodynamics simulations. Microscopic theory of interstitial solid solutions was developed about four decades ago by Khachaturyan (see Ref. 17 and references therein) within the concentration wave theory. The essential ingredient of this theory is the Krivoglaz-Kanzaki-Khachaturyan model (KKKM) for the strain-induced interactions,[18] which originate from large local lattice distortions around interstitial atoms. It has been believed for a long time that they, in fact, play a dominant role in the interstitial ordering. The chemical parts of interactions between interstitials were considered to be short range and used as a fitting parameter to existing experimental data.[2,19–22]

In our investigation, both of these interactions, chemical and strain induced, will be obtained by the state-of-the-art first-principles techniques based on density-functional theory (DFT).[23] Let us note that the latter has become possible only recently with the advent of computers. One of the first *ab initio* investigations of the carbon-carbon interactions and the phase stability in cubic TiC_x system was performed by Korzhavyi *et al.*[24] in 2002. The carbon-carbon interactions in bcc Fe have been recently calculated by Domain *et al.*[25,26] Tao *et al.*[27] calculated the relative stability of some set of ordered hydrogen interstitial structures in hcp Ti and Mg.

II. METHODOLOGY

A. Configurational Hamiltonian

We assume that interstitial-interstitial interactions are independent of their configuration or their distribution in the interstitial sites, and thus their configurational energetics can be studied within the Ising model for a two component alloy of occupied and vacant interstitial sites. The corresponding Hamiltonian is

$$H = \frac{1}{2}\sum_{p}\sum_{i,j\subset p} V_p^{(2)}\delta x_i \delta x_j + \frac{1}{3}\sum_{t}\sum_{i,j,k\subset t} V_t^{(3)}\delta x_i \delta x_j \delta x_k + \cdots . \tag{1}$$

Here, $V_p^{(2)}$ and $V_t^{(3)}$ are the effective two- and three-site interactions for the corresponding coordination shell, p, and triangle, t; $\delta x_i = x_i - \langle x_n \rangle$ is the deviation of the occupation numbers, where x_i is from its average value, $\langle x_n \rangle = x$, and x_i takes on values 1 if site i is occupied by an interstitial atom and 0 otherwise. The concentration and volume dependence of interactions are assumed here.

B. Effective interactions

The effective cluster interactions describe a response of the system to a given rearrangement of atoms on the lattice under given external conditions, and thus they are temperature dependent due to, for instance, contribution from the electronic and vibrational thermal excitations, which depend on the alloy configuration. However, we will neglect these effects, assuming that the chemical, $V_p^{(2)\text{-}ch}$, and strain-induced, $V_p^{(2)\text{-}si}$, interactions are dominant in this case, and the whole effective interaction is given by their sum, $V_p^{(2)} = V_p^{(2)\text{-}ch} + V_p^{(2)\text{-}si}$. Here, the chemical part of the effective interaction is associated with certain configurational energy due to the redistribution of the atoms in the ideal (undistorted) lattice positions. The subsequent local relaxations, minimizing the elastic energy, then give rise to the strain-induced interactions. The chemical interactions are, in general, multisite due to the quantum-mechanical nature of the interatomic bonding, while the strain-induced interactions are pairwise in the (quasi)harmonic approximation for the lattice force constants, which will be assumed in this work.

The effective interactions can be calculated by different first-principles methods. If the pair interactions are dominating, which is the case of the systems considered in this paper, the most straightforward way to obtain the chemical part of the effective cluster interactions in the dilute limit is to calculate the total energies of two large supercells: one where two interstitials are in position of a given coordination shell and the other one, where they are far enough to prevent their interaction. The lattice positions, of course, should be fixed and the same in both calculations. If the size of the supercell is not large enough to provide the isolation of the two interstitials, the effective cluster interaction can be obtained in equivalent calculations of three supercell as[28,29]

$$V_p^{(2)} = E_{2,p} + E_0 - 2E_1 . \tag{2}$$

Here, E_0, E_1, and $E_{2,p}$ are the total energies (per cell) of supercells (of the same size) without interstitials, with one interstitial atom and two interstitial atoms at the pth coordination shell. As has been mentioned, if all the atoms are in the ideal lattice and interstitial positions, this formula yields the chemical contribution to the effective pair interaction at the pth coordination shell, $V_p^{(2)\text{-}ch}$. If all the atomic positions are relaxed (note, however, that the translation vectors, i.e., the global geometry and the volume of the system, should be fixed), $V_p^{(2)}$ is the total effective interaction. This means that the strain-induced interactions can be obtained as the differ-

ence of $V_p^{(2)}$ and $V_p^{(2)\text{-}ch}$, which is, in fact, just the difference of relaxation energies of two impurities and a single impurity,

$$V_p^{(2)\text{-}si} = E_{2,p}^{rel} - 2E_1^{rel}. \quad (3)$$

There are two drawbacks of this method. First of all, it yields interactions in the dilute limit, although, strictly speaking, the interactions defined in Eq. (2) are concentration independent, since it is based on the total energies of the systems having different compositions. However, in the dilute limit, when the size of the supercell is large enough, one can neglect the small difference of the concentrations. The other drawback is the fact that it can only be used for few several nearest-neighbor interactions due to the limitations of the size of the supercell in the total-energy calculations.

The method, which can be used as complementary in order to obtain the long-range chemical effective interactions as well as multisite interaction, is the screened generalized perturbation method (SGPM).[30,31] The starting point in the SGPM is the electronic structure of a random alloy for a given composition and external conditions obtained in the coherent-potential approximation (CPA).[32–34] As soon as it is known, the one-electron contribution to the effective cluster interaction of any type can be determined by using perturbation technique, which leads to a simple analytical expression in terms of multiple-scattering theory quantities known from the corresponding electronic structure calculations. This means that the SGPM allows one to determine any given effective cluster interaction, pairwise, or multisite.

The main drawback of the SGPM is its reduced accuracy in the case of alloys where either there is large charge transfer between alloy components or the CPA error is too large. The first error, however, is relevant only for the effective pair interactions, which have an additional electrostatic contribution given by the screened Coulomb interactions.[31,35] The problem here is due to the use of the atomic sphere approximation (ASA) for the one-electron density and potential, which is usually used in the CPA-based methods. Nevertheless, since the screened electrostatic interactions are usually short range, the tail or the long-range part of the pair effective interactions is usually reproduced quite accurately.

As for the CPA error, it is system dependent. In the case of interstitial alloys, where an alloy is formed by vacant interstitial sites (vacancies) and solute atoms (oxygen, nitrogen), it may be large. However, since it is related to the so-called local environment effects in the electronic structure, it affects mostly the nearest-neighbor interactions, where the local environment effects are mostly pronounced. Anyway, the answer to the question if the method is applicable to a particular system or not can be given only by applying this method and checking its results, for instance, by comparing the SGPM interactions with those obtained by other more accurate methods. As has been demonstrated in Ref. 24 in the study of phase equilibria in the cubic TiC_x interstitial ordered alloys, the SGPM works well in this kind of systems.

As for the strain-induced interactions, their long-range tail can also be estimated within the first-principles calculations assuming that local atomic displacements are small and thereby only harmonic contribution is important. In this case, the force acting on a host atom due to two interstitials and the resulting displacement can approximately be given by a superposition of the forces and displacements produced by each interstitial atom. Thus, using the Hellmann-Feynman forces from the first-principles calculations of the host atoms around a *single* impurity, $\mathbf{F}_i$ (before relaxation), local displacements of the host atoms, $\mathbf{u}_i$ (after relaxations), and definition (3), one can arrive to the following equation for the strain-induced interactions in such a superposition model (SM):

$$V_p^{(2)\text{-}si} = -\frac{1}{2}\sum_i [(\mathbf{F}_i^1 + \mathbf{F}_i^2)(\mathbf{u}_i^1 + \mathbf{u}_i^2) - \mathbf{F}_i^1\mathbf{u}_i^1 - \mathbf{F}_i^2\mathbf{u}_i^2]. \quad (4)$$

Here, the summation is performed over all the host atoms and $\mathbf{F}_i^{1(2)}$ and $\mathbf{u}_i^{1(2)}$ are the forces and displacements induced either by the first (1) or second (2) interstitial atom, respectively.

TABLE I. Experimental (room temperature) (Ref. 40) and theoretical (0 K) lattice parameters (in Å) of pure metals.

	Ti	Zr	Hf
		Experiment	
a	2.9511	3.2321	3.1971
c	4.6843	5.1477	5.0606
		Theory	
a	2.9317	3.2370	3.2035
c	4.6444	5.1831	5.0589

C. Details of calculations

The supercell total-energy calculations for the chemical and total effective pair interactions according (2) have been performed by the projector augmented-wave (PAW) method[36] as is implemented in the Vienna *ab initio* simulation package (VASP).[37] The generalized gradient approximation[38] has been used for the exchange-correlation energy. The energy cutoff was 500 eV. Other details of the supercell calculations are as follows. Two hcp supercells, containing 54 atoms ($3\times3\times3$ hcp unit cells) and 200 atoms ($5\times5\times4$), have been used. The Monkhorst-Pack grid[39] with subdivisions along each reciprocal-lattice vector $2\times2\times2$ and $6\times6\times6$ has been used in the 200- and 54-atom supercell calculations, respectively. The total-energy calculations have been carried out at theoretical equilibrium lattice constants of supercells with one interstitial atom.

The theoretical lattice constants for pure metals are listed in Table I together with the corresponding experimental data.[40] As one can see the agreement between theory and experiment is as usual quite reasonable. In Table II we show the concentration lattice expansion coefficients obtained in the single-impurity calculations for the 54-atom supercell together with experimental data.[40] The agreement between theory and theoretical results is satisfactory, taking into con-

TABLE II. Experimental (room temperature) (Ref. 40) and theoretical values (0 K) of the concentration expansion coefficients, $L_{xx}=\frac{1}{a}\frac{da}{dx}$ and $L_{zz}=\frac{1}{c}\frac{dc}{dx}$, of oxygen and nitrogen interstitial solid solutions.

	Ti		Zr		Hf	
	O	N	O	N	O	N
			Experiment			
L_{xx}	0.027	0.054	0.037	0.031	0.025	
L_{zz}	0.085	0.171	0.038	0.062	0.040	
			Theory			
L_{xx}	0.049	0.065	0.050	0.059	0.024	0.042
L_{zz}	0.084	0.087	0.034	0.024	0.103	0.104

sideration that these coefficients should depend on the interstitial configuration and they are obviously different in the single-impurity calculation and concentrated interstitial alloys investigated in the experiment.

The SGPM effective interactions have been calculated by the exact muffin-tin orbital method.[41] In this case the interstitial sublattice has been treated as a random alloy of interstitial atoms and vacant positions using the CPA. The corresponding on-site and intersite screening constants for the screened Coulomb interactions have been obtained in the locally self-consistent Green's function calculations as described in Ref. 35. The atomic sphere radii ratio of the host and oxygen (interstitial) sublattices has been chosen to be 1.5, which minimizes the error due to the ASA by providing the close values of the one-electron potentials of the metal host and the empty spheres of the interstitial sites at the atomic sphere radii. For such a ratio, the on-site screening constant for the oxygen-vacancy alloy on the interstitial sublattice was 1.0 in the single-site DFT-CPA calculations.[35]

Let us also note that the multipole moment correction to the one-electron potential and energy has been used in the calculations.[35,42] As has been shown,[31,35] the latter provides the accurate configurational energetics of the alloys on the ideal lattice as in the total-energy calculations as well as in the case of the SGPM interactions.

III. EFFECTIVE INTERACTIONS OF INTERSTITIALS

The octahedral interstitial sites form a simple hexagonal lattice in the hcp structure (see Fig. 1). Detailed information about the coordination shells of interstitial sites is given in Table III.

A. Effective chemical oxygen-oxygen interactions

In Fig. 2 we present the chemical part of the effective pair interactions obtained in the 200- and 54-atom supercell calculations using Eq. (2) and by the SGPM. One can see that the agreement between supercell calculations is quite good, which means that the 200-atom supercell is large enough to produce the quantitatively accurate results at least for the first several coordination shells. It is also clear that both methods produce very close results, so the SGPM can indeed be used for the assessments of the long-range chemical effective pair interactions.

The characteristic feature of the chemical effective interactions in all the systems is the large positive interactions at the first two coordination shells, especially at the first one. This means that oxygen atoms strongly repel each other at the first two coordination shells, i.e., when oxygen atoms are next to each other in the $(1\bar{2}10)$ and (0001) planes. At the same time, the chemical interactions are relatively short range: more distant interactions are several orders of magnitude less than those at the first two coordination shells. This validates the use of a restricted set of the effective pair interactions in the configurational Hamiltonian, at least in the cases where it does not concern the stability of long period superstructures, whose formation can be affected by the so-called Fermi-surface effects leading to a specific contribution from the long-range effective interactions.

Another important point concerns the multisite effective interactions. As has been noted, Eq. (2) is valid only if the contribution from the multisite interactions can be neglected. The strongest multisite interaction found in the SGPM calculations is for the triangle formed by the sides, which correspond to the first, second, and third coordination shells of the octahedral interstitial positions. In TiO alloys it is about 0.63 mRy, while in ZrO and HfO it is 0.42 mRy. These values are one order of magnitude less than the correspond-

TABLE III. Coordination shells of the octahedral interstitial sites.

N	lmn	d
1	001	$c/2$
2	100	a
3	101	$(a^2+c^2/4)^{1/2}$
4	002	c
5	110	$a\sqrt{3}$
6	102	$(a^2+c^2)^{1/2}$
7	111	$(3a^2+c^2/4)^{1/2}$
8	200	$2a$
9	201	$(4a^2+c^2/4)^{1/2}$
10	112	$(3a^2+c^2)^{1/2}$

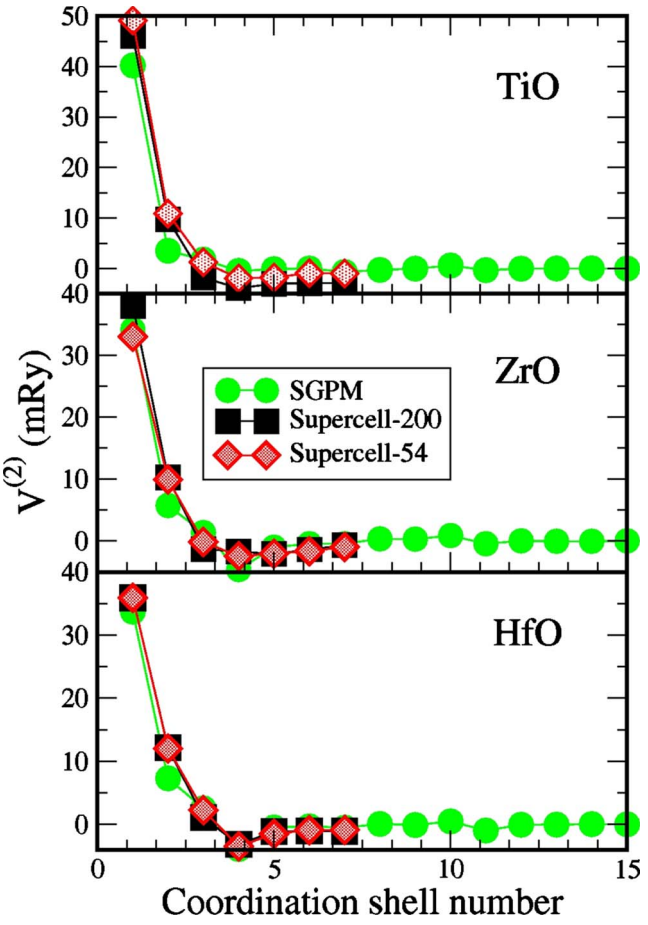

FIG. 2. (Color online) Chemical part of the effective pair interactions of the oxygen interstitial alloys in Ti (upper panel), Zr (middle panel), and Hf (lower panel) obtained in the 200- and 54-atom supercell calculations by the PAW method and SGPM.

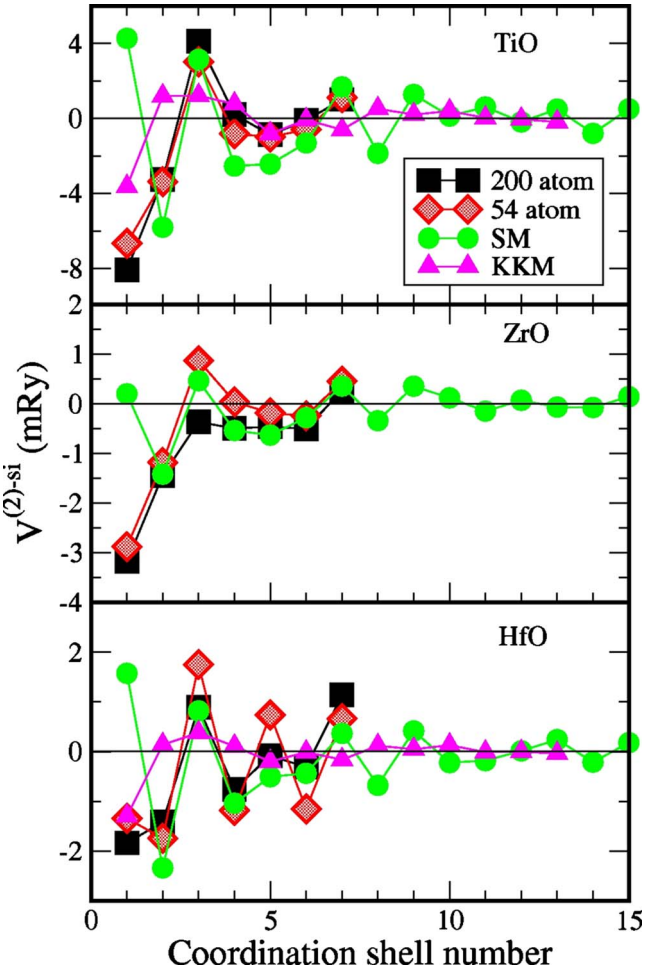

FIG. 3. (Color online) Strain-induced interactions of oxygen atoms in Ti (upper panel), Zr (middle panel), and Hf (lower panel) obtained in the 200- and 54-atom supercell calculations from Eq. (3) as well as in the SM and phenomenological KKKM (Ref. 43).

ing pair effective interactions at the first three coordination shells and therefore they cannot influence the ordering of oxygen. This also means that the concentration dependence of the effective interactions is relatively weak and the supercell calculations should produce reliable results for the interactions.

B. Strain-induced oxygen-oxygen interactions

The results of the calculations for the oxygen-oxygen strain-induced interactions by different methods are presented in Fig. 3. The strain-induced interactions have been obtained in the direct calculations using Eq. (3) for the 54- and 200-atom supercells as well as using superposition model given by Eq. (4). In the latter case, we have used the forces and displacements of the host atoms up to the 13th coordination shell, which have been determined in the single-impurity calculations of the 200-atom supercell. It is clear that the size of the supercell affects the strain-induced interactions in a relatively higher degree than in the case of the chemical interactions. This can be due to the long-range nature of the strain effect, which appears to be much more suppressed due to the periodic boundary conditions in the small supercell. Nevertheless, the difference is not that large to affect the simulation results.

One can also see that the strain-induced interactions given by the SM are in reasonable agreement with directly obtained in the supercell calculations. The only exception is the strain-induced interactions at the first coordination shell. The failure of the SM to produce the nearest-neighbor strain-induced interaction is due to the fact that this model does not take into consideration the direct elastic interaction between interstitials themselves, which is quite large when they are next to each other. Moreover, the superposition approach is also violated in this case: both the displacements and forces of the host atoms around the two close to each other interstitial atoms are different from the sum of the forces and displacements produce by each interstitial atom.

In Fig. 3 we also show the results for the strain-induced interactions obtained by Blanter *et al.* in Ref. 43 within the phenomenological KKKM,[17,18,44] which has been frequently used in the past. The force constants or dynamical matrix of the host metal and the concentration lattice expansion coefficients, related to static atomic displacements in the continuous consideration, are used in this model to determine the

TABLE IV. Effective pair interactions (in mRy), $V_p^{(2)}$, of oxygen interstitial alloys in hcp Ti, Zr, and Hf obtained in the 200-atom supercell calculations. The values in parentheses are from the 54-atom supercell calculations.

N	*lmn*	Ti-O	Zr-O	Hf-O
1	001	38.00 (42.47)	34.85 (30.16)	34.06 (34.54)
2	100	6.48 (7.54)	8.84 (8.86)	10.74 (10.27)
3	101	2.28 (4.29)	−1.67 (0.72)	1.97 (4.02)
4	002	−3.68 (−2.72)	−2.18 (−2.43)	−3.93 (−4.67)
5	110	−3.86 (−2.76)	−2.58 (−2.22)	−1.23 (−0.76)
6	102	−3.02 (−1.50)	−1.87 (−1.90)	−1.33 (−2.08)
7	111	−1.82 (0.13)	−0.41 (−0.51)	0.07 (−0.21)

strain-induced interactions. All these parameters are deduced from the available experimental data.[43] It is clear that the KKKM does not describe properly the strain-induced interactions in these alloys. Of course, it does not mean that it is not valid at all because the presented results are specific for the approximations and assumptions adopted in Ref. 43. However, this result shows that one really needs a first-principles theory when it comes to quantitative modeling of the interatomic interactions.

In contrast to the chemical part of the effective pair interactions, the strain-induced interactions are negative at the first two coordination shells; i.e., the local lattice relaxations around two interstitial atoms in the corresponding positions lead to their mutual attraction. However, it is clear that it is much weaker than the strong chemical repulsion. One can also see that the strain-induced interactions decay very slowly with the distance giving a substantial contribution to the effective pair interactions at the distant coordination shells.

C. Total effective interactions of oxygen and nitrogen interstitials

The first seven total effective pair interactions of oxygen interstitials obtained in the PAW supercell calculations are shown in Table IV. One can see that the size of the supercell has a pronounced effect on the interactions starting from the third coordination shell, which is especially large in the case of the Ti-O interstitial alloys. In the case of the Zr-O alloys, the interaction at the third coordination shell is positive in the 54-atom supercell calculations (repulsion of interstitial atoms), while it is negative (attraction of the interstitial atoms) in the 200-atom supercell calculations. Such a dependence on the size is mainly due to the strain-induced interactions. Unfortunately, we could not use larger supercells due to exceeding computational demands. Nevertheless, the observed differences are not so dramatic. In particular, we find the same ground-state structures in Zr-O alloys independently if we use the 54-atom or 200-atom supercell interactions. Thus, we believe that the 200-atom supercell interactions should produce a qualitatively correct picture of the interstitial ordering.

In order to test the effective pair interactions, we have calculated the oxygen activity coefficients in hcp Hf using the 200-atom supercell interactions. The results are presented in Fig. 4 together with the experimental data from Refs. 45 and 46. The calculations have been done by the method described in Refs. 47 and 48. The theoretical and experimental values of the oxygen activity are normalized by the maximal experimental oxygen activity, a_{exp}^{max}, for the maximum investigated oxygen concentration in the interstitial sites, 21 at. %. It is clear that the agreement between theoretical and experimental data is very good. Similar results have also been obtained for the oxygen activity in hcp Zr and Ti, although the agreement with the experimental data was slightly worse.

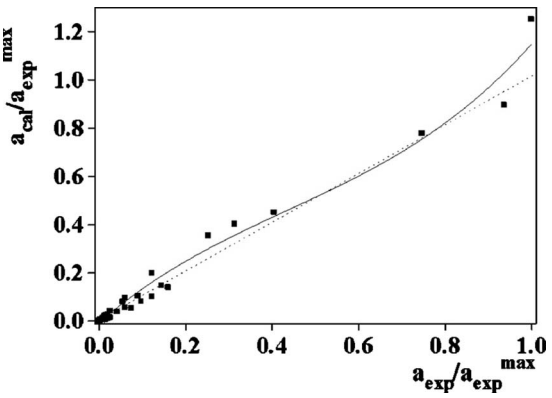

FIG. 4. Comparison of the calculated (solid line) and experimental (filled squares) oxygen activity in hcp Hf.

The effective interactions of nitrogen interstitial alloys obtained in the 200-atom supercell calculations are shown in Table V. They exhibit the behavior very similar to that effective interactions in oxygen interstitial alloys: a very strong repulsion at the first two coordination shells and quite strong attraction for the more distant coordination shells. This means that the nitrogen atoms in group-IV metals should form ordered structures similar to those formed in the oxygen alloys.

IV. INTERSTITIAL ORDERING

The effective pair interactions obtained in the 200-atom supercell calculations have been used in the Monte Carlo simulations in order to determine the ordered structures and transition temperatures of the oxygen and nitrogen interstitials. In doing so, we have neglected the following effects:

TABLE V. Effective pair interactions (in mRy), $V_p^{(2)}$, of nitrogen atoms in hcp Ti, Zr, and Hf.

N	*lmn*	Ti-N	Zr-N	Hf-N
1	001	31.10	31.10	25.59
2	100	1.84	5.34	5.62
3	101	−0.78	−1.46	0.40
4	002	−1.11	−0.58	−1.01
5	110	−2.10	−1.56	−1.62
6	102	−1.79	−0.76	−1.78
7	111	−1.01	−0.46	−0.95

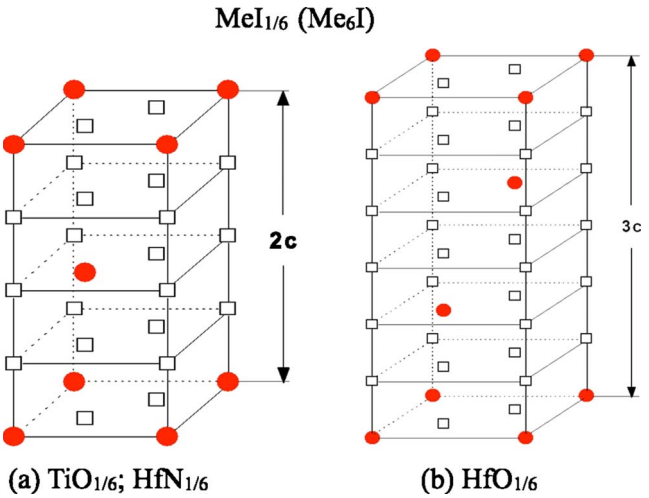

FIG. 5. (Color online) The ground-state structures of the $MeI_{1/6}$ interstitial alloys. Only interstitial positions are shown. Filled symbols are oxygen atoms in the interstitial positions.

(1) the renormalization of the interactions due to thermal lattice expansion; (2) the contribution to the configurational thermodynamics from lattice vibrations; and (3) the concentration dependence of the effective interactions, which combines two effects: the concentration lattice expansion and electronic structure renormalization. Besides, the results, which will be presented below, are obtained without the multisite effective cluster interactions and long-range effective pair interactions obtained by the SGPM and SM.

In fact, we have found that the multisite and long-range effective pair interactions may change the transition temperatures within 10–15 %. However, the ordered structures remain the same, which means that the first seven interactions reproduce the qualitative picture of the ordering. Let us note that the long-range effective pair and multisite interactions contribute in some way to the effective pair interactions obtained in the supercell calculations. This means that a special care should be taken to include the interactions obtained by different methods. The neglect of the thermal and concentration lattice expansions should lead to the overestimation of the ordering temperatures. However, the accurate description of the phase equilibria, including the phase diagrams of these systems, requires the calculation of the free energy of different phases and it is beyond the scope of the present paper.

The Monte Carlo calculations have been done for several different occupations of the interstitial sites, including 1/6, 1/3, and 1/2, which correspond to the stoichiometric compositions of the observed ordered structures. The size of the supercell has been varied from $12\times12\times12(\times2)$ to $24\times24\times24(\times2)$, but it has little effect on the transition temperatures and no effect on the resulting ground-state structures.

A. Oxygen ordering

In Fig. 5–7 we show the ground-state ordered structures of oxygen and nitrogen interstitials in the IVB transition metals determined in the Monte Carlo calculations. In the case of

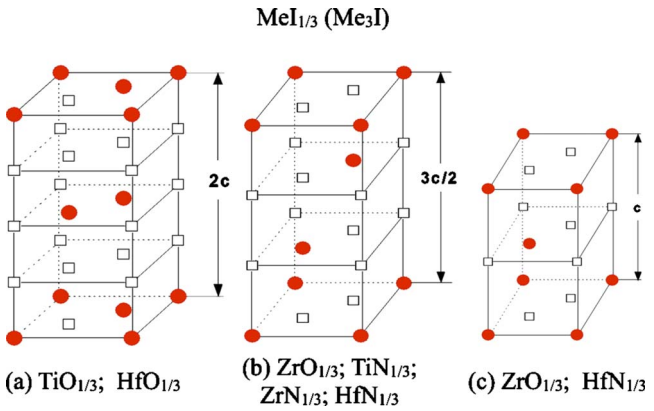

FIG. 6. (Color online) Ground-state structures of $MeI_{1/3}$ interstitial alloys.

oxygen interstitials, the theory reproduces all the experimentally known ordered structures in the hcp Ti and Hf (Refs. 1 and 6): $TiO_{1/6}$, $TiO_{1/3}$, $TiO_{1/2}$, $HfO_{1/6}$, and $HfO_{1/3}$. The occupation of the interstitial sites in these structures can be understood in terms of the competition between different effective pair interactions and the availability of the interstitial positions, which changes with the oxygen concentration. There is, however, one common feature for all the structures: the nearest-neighbor interstitial positions of oxygen atoms are vacant. This is apparently due to the extremely strong repulsion of oxygen and nitrogen atoms at the first coordination shell, which has been identified above as "chemical" effect.

One can notice that the oxygen ordered structures in Zr are different from those in Ti and Hf. This is mainly due to the effective interaction at the third coordination shell, which is negative, i.e., attractive, in Zr, while it is positive and relatively large in Ti and Hf. The possibility of oxygen atoms occupy the third coordination shell in Zr results in the appearance of oxygen atoms in every (0001) layer, which contrasts with the ordering of oxygen in Ti and Hf, where they occupy only every second layer.

The calculated ground-state structure of ZrO_x alloys for $x<1/3$ is given by a mixture of pure Zr and $ZrO_{1/3}$ (b) shown in Fig. 6. At the same time, as has been found in the neutron-diffraction study by Arai and Hirabayashi,[10] the structure of $ZrO_{1/6}$ is isomorphic with that of $TiO_{1/6}$ [Fig.

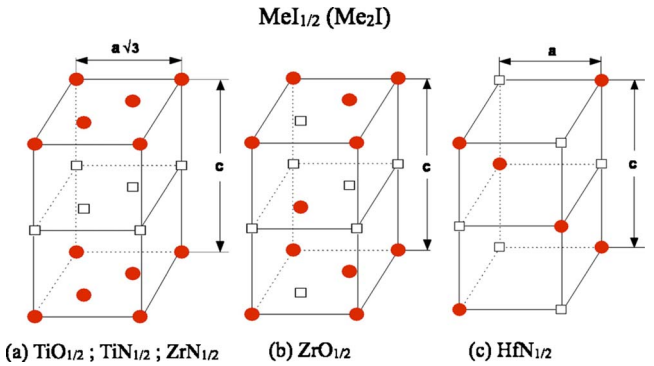

FIG. 7. (Color online) Ground-state structures of $MeI_{1/2}$ interstitial alloys.

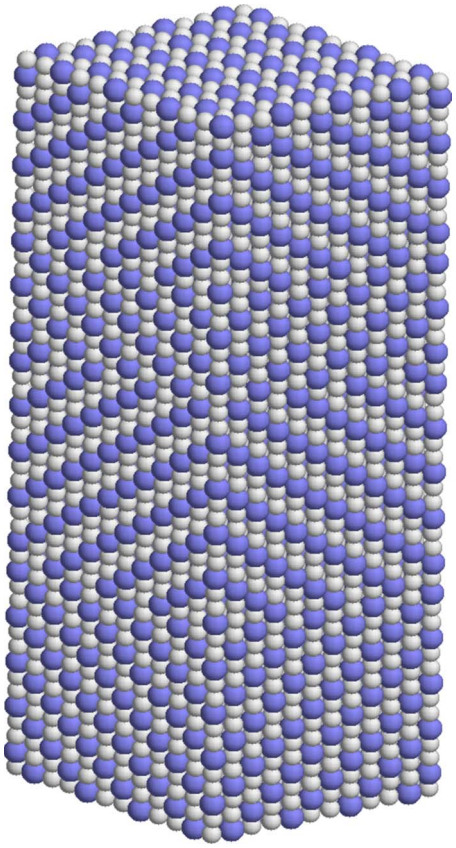

FIG. 8. (Color online) A snapshot of a low-temperature structure of $ZrO_{1/3}$ obtained in the Monte Carlo simulations. Filled symbols are oxygen atoms in the interstitial positions.

5(a)]. However, the neutron-diffraction pattern consists of peaks related to the $TiO_{1/6}$ as well as to the $ZrO_{1/3}$ (b) structures; i.e., oxygen atoms do not form homogeneously ordered structure. This discrepancy between the theory and experiment is most probably due to the fact that the sensitivity of effective interaction at the third coordination shell basically determines the stability of $ZrO_{1/3}$ (b) structure to the details of the calculation, such as the size of the supercell. Since this interaction is relatively small, it can also be affected by different factors such as concentration or lattice parameter. The lattice vibrations can also be important for the accurate thermodynamic simulations in this case.

Let us note that it is very difficult (we have not been actually able) to produce the $ZrO_{1/3}$ (b) structure, presented in Fig. 6(b) in the Monte Carlo simulations. The resulting structure is a combination of the $ZrO_{1/3}$ (b) structure but with alternating sequences of oxygen layers, *ABC* and *ACB*, divided by the "antiphase" boundary, $ZrO_{1/3}$ (c), presented in Fig. 6(c). In Fig. 8 we show the snapshot obtained in one of the Monte Carlo simulations. This is, in fact, in agreement with the existing experimental data,[8] according to which the LPS of this type exists for the oxygen occupation close to this composition with a relatively short period, about several layers. At the same time, the theoretical period strongly depends on the computational details, reflecting that it is nonequilibrium nature. It is quite possible that the accurate theoretical description of the LPS requires the use of not only more accurate models for the effective interactions but also consideration of the specific inhomogeneous lattice distortions due to the existence of the "antiphase boundaries." If the oxygen composition in the octahedral sites exceeds 1/3, an additional structure precipitates in the Monte Carlo simulations, $ZrO_{1/2}$, as shown in Fig. 7(b).

TABLE VI. Order-disorder transition temperatures (in K) of oxygen interstitials.

Phase	Theory	Experiment
$TiO_{1/6}$	1200	700
$TiO_{1/3}$	2120; 1300	780; 850
$TiO_{1/2}$	2860	
$ZrO_{1/3}$	1430; 900	810
$HfO_{1/6}$	600	730
$HfO_{1/3}$	1300; 860	

In Table VI we show the calculated transition temperatures for five oxygen alloys. The transition temperatures are about twice as high as experimental data for the interstitial oxygen alloys in Ti. There can be many reasons for such spectacular disagreement. Among them is the neglected vibrational contribution in this work, which can be quite large due to small mass of interstitials. We also use zero-temperature theoretical values for the lattice parameters, which take into consideration neither thermal lattice expansion nor quite strong concentration lattice expansion existing in these alloys. Let us note in this respect that the negative (attractive) effective interactions have the strongest effect on the ordering temperature. It is quite clear if one compares the transition temperatures and effective interactions for Ti and Hf: the strongest repulsive interactions at the first coordination shell are practically the same. This means that the transition temperature is strongly affected by the sign and the values of more distant interactions. Let us also note that the case of the $MeO_{1/3}$ alloys, two ordering transitions, occurs, which is in agreement with existing experimental and theoretical analyses.

B. Nitrogen ordering

As has been mentioned, the effective interactions in the nitrogen alloys (see Table V) are similar to those in oxygen alloys. In particular, the effective interactions at the first and second coordination shells are very strong and repulsive, while the interactions at more distant coordination shells are attractive. The interactions at the third coordination shell are now negative (attractive) in the Ti-N and Zr-N interstitial alloys and positive in Hf-N. This means that the ordering of nitrogen in Ti and Zr should be similar to that of oxygen one in Zr. This is indeed the case, as one can see in Figs. 5–7, where we show the ground-state structures of nitrogen interstitial solid solutions in hcp Ti, Zr, and Hf obtained in the Monte Carlo simulations. As in the case of ZrO system, there are no stable stoichiometric ordered structures in $TiN_{1/6}$ and $ZrN_{1/6}$: their ground state is formed by the mixture of pure metals and $TiN_{1/3}$ and $ZrN_{1/3}$, which have exactly the same structure as $ZrO_{1/3}$.

TABLE VII. Order-disorder transition temperatures of nitrogen interstitial alloys.

Phase	T_c (K)
$TiN_{1/3}$	1700, 660
$TiN_{1/2}$	860
$ZrN_{1/3}$	1200; 820
$ZrN_{1/2}$	2020
$HfN_{1/6}$	550
$HfN_{1/3}$	1700; 820
$HfN_{1/2}$	770

In this respect, it is interesting to consider the nitrogen ordered structures in Hf. Up to 30 at. % of nitrogen can be dissolved in Hf, however, there is no experimental information about ordered phases. The effective pair interaction at the third coordination shell is positive in this case, and, as a result, the ground-state structure of $HfN_{1/6}$ is the same as in the case of $TiO_{1/6}$. However, the ground-state structure of $HfN_{1/3}$ is equivalent to that of $ZrO_{1/6}$, where oxygen atoms occupy every (0001) plane of the interstitial positions. This is of course due to the fact that the value of the interaction at the third coordination shell is quite small, so it does not play the decisive role in the final energy balance.

Finally, In Table VII we show the transition temperatures for the ordered nitrogen interstitials. In the case of $MeN_{1/3}$ compositions, two ordering transitions are observed in the Monte Carlo simulations. Let us note, however, that the heat capacity has a very shallow maximum at the high-temperature transition, unusual for the usual phase transitions. Obviously, an additional investigation is needed to clarify the details of this phenomenon, which is beyond the scope of the present investigation.

V. CONCLUSIONS

The ordering of interstitial oxygen and nitrogen in hcp Ti, Zr, and Hf has been investigated theoretically in the statistical thermodynamics simulations by the Monte Carlo method with the effective interactions obtained in the state-of-the-art first-principles calculations. For oxygen interstitial alloys, we obtain all the experimentally observed ordered structures but $ZrO_{1/6}$, for which the experimental information is actually not certain. There is no experimental information about ordered structures in nitrogen interstitial alloys, and we predict that nitrogen ordering should be similar to that of oxygen.

Although it is clear that the obtained interactions provide physically correct picture of the ordering phenomena, an additional investigation is needed to find the role of concentration and temperature dependence of the interactions, as well as vibrational effects. The calculations, which take these effects into consideration, can finally lead to the complete and accurate theoretical description of the phase equilibria in these systems.

ACKNOWLEDGMENTS

A.V.R. is grateful to the Swedish Research Council (VR) and the Swedish Foundation for Strategic Research (SSF) for financial support. M.S.B. and V.V.D. acknowledge the financial support of Russian Federal Education Agency under Contract No. P2291 and Russian Found of Fundamental Researches under Grant No. 10-2-00176. Calculations have been done using UPPMAX (Uppsala), PDC (Stockholm), and NSC (Linköping) resources provided by the Swedish National Infrastructure for Computing (SNIC).

[1] T. Tsuji, J. Nucl. Mater. **247**, 63 (1997).
[2] M. S. Blanter and A. G. Khachaturyan, Metall. Trans. A **9A**, 753 (1978).
[3] V. A. Somenkov, A. V. Irodova, and S. Sh. Shilshtein, Solid State Phys. **20**, 3076 (1978).
[4] B. Holmberg, Acta Chem. Scand. **16**, 1245 (1962).
[5] S. Yamaguchi, J. Phys. Soc. Jpn. **27**, 155 (1969).
[6] M. Koiwa and M. Hirabayashi, J. Phys. Soc. Jpn. **27**, 801 (1969).
[7] S. Yamaguchi, K. Hiraga, and M. Hirabayashi, J. Phys. Soc. Jpn. **28**, 1014 (1970).
[8] S. Yamaguchi, J. Phys. Soc. Jpn. **24**, 855 (1968).
[9] S. Hashimoto, H. Iwasaki, S. Ogawa, S. Yamaguchi, and M. Hirabayashi, J. Appl. Crystallogr. **7**, 67 (1974).
[10] T. Arai and M. Hirabayashi, J. Less-Common Met. **44**, 291 (1976).
[11] T. Tsuji, M. Amaya, and K. Naito, J. Therm. Anal. **38**, 1817 (1992).
[12] T. Tsuji and M. Amaya, J. Nucl. Mater. **223**, 33 (1995).
[13] M. Hirabayashi, S. Yamaguchi, and T. Arai, J. Phys. Soc. Jpn. **35**, 473 (1973).
[14] B. Holmberg, Acta Chem. Scand. (1947-1973) **16**, 1255 (1962).
[15] Kubaschewski-von Goldbeck, At. Energy Rev. **6**, 98 (1976).
[16] H. Okamoto, Bull. Alloy Phase Diagrams **12**, 146 (1990).
[17] A. G. Khachaturyan, *Theory of Structural Transformations in Solids* (Wiley, New York, 1983).
[18] M. A. Krivoglaz, *X-ray and Neutron Diffraction in Nonideal Crystals* (Springer, Berlin, 1995); *Diffuse Scattering of X-Rays and Neutrons by Fluctuations* (Springer, Berlin, 1996).
[19] M. Ivasishin, N. S. Kosenko, S. V. Shevchenko, V. A. Tatarenko, and C. L. Tsynman, Metalophysica Novejshie Technologii **19**, 8 (1997) (in Russian).
[20] M. S. Blanter, I. S. Golovin, E. B. Granovsky, and H.-R. Sinning, J. Alloys Compd. **345**, 1 (2002).
[21] A. G. Khachaturyan, *Theory of Phase Transformation and Structure of Solid Solutions* (Nauka, Moscow, 1974) (in Russian).
[22] V. N. Bugaev and V. A. Tatarenko, *Interaction and Arrangement of Atoms in Interstitial Solid Solutions Based on Closed-Packed Metals* (Naukova Dumka, Kiev, 1989) (in Russian).
[23] P. Hohenberg and W. Kohn, Phys. Rev. **136**, B864 (1964); W. Kohn and L. J. Sham, *ibid.* **140**, A1133 (1965).
[24] P. A. Korzhavyi, L. V. Pourovskii, H. W. Hugosson, A. V. Ruban,

and B. Johansson, Phys. Rev. Lett. **88**, 015505 (2001).
[25] C. Domain, C. S. Becquart, and J. Foct, Phys. Rev. B **69**, 144112 (2004).
[26] C. Domain, J. Nucl. Mater. **351**, 1 (2006).
[27] S. X. Tao, P. H. L. Notten, R. A. van Santen, and A. P. J. Jansen, Phys. Rev. B **79**, 144121 (2009).
[28] T. Hoshino, W. Schweika, R. Zeller, and P. H. Dederichs, Phys. Rev. B **47**, 5106 (1993).
[29] A. V. Ruban and I. A. Abrikosov, Rep. Prog. Phys. **71**, 046501 (2008).
[30] F. Ducastelle and F. Gautier, J. Phys. F: Met. Phys. **6**, 2039 (1976).
[31] A. V. Ruban, S. Shallcross, S. I. Simak, and H. L. Skriver, Phys. Rev. B **70**, 125115 (2004).
[32] P. Soven, Phys. Rev. **156**, 809 (1967).
[33] D. W. Taylor, Phys. Rev. **156**, 1017 (1967).
[34] B. L. Gyorffy, Phys. Rev. B **5**, 2382 (1972).
[35] A. V. Ruban and H. L. Skriver, Phys. Rev. B **66**, 024201 (2002); A. V. Ruban, S. I. Simak, P. A. Korzhavyi, and H. L. Skriver, *ibid.* **66**, 024202 (2002).
[36] P. E. Blöchl, Phys. Rev. B **50**, 17953 (1994).
[37] G. Kresse and J. Hafner, Phys. Rev. B **48**, 13115 (1993); G. Kresse and J. Furthmüller, Comput. Mater. Sci. **6**, 15 (1996).
[38] J. P. Perdew, K. Burke, and M. Ernzerhof, Phys. Rev. Lett. **77**, 3865 (1996).
[39] H. J. Monkhorst and J. D. Pack, Phys. Rev. B **13**, 5188 (1976).
[40] *Phase Equilibria, Crystallographic and Thermodynamic Data of Binary Alloys*, Landolt-Börnstein, New Series, Group 4: Physical Chemistry Group IV, Physical Chemistry, Vol. 5 (Springer-Verlag, Berlin, 1994).
[41] L. Vitos, Phys. Rev. B **64**, 014107 (2001); L. Vitos, I. A. Abrikosov, and B. Johansson, Phys. Rev. Lett. **87**, 156401 (2001).
[42] A. V. Ruban and H. L. Skriver, Comput. Mater. Sci. **15**, 119 (1999).
[43] M. S. Blanter, A. V. Ruban, and V. V. Dmitriev, J. Phys. Chem. Solids.
[44] V. A. Tatarenko and C. L. Tsynman, Metalophysica Novejshie Technologii **19**, 9 (1997) (in Russian).
[45] K. L. Komarek and M. Silver, *Proc. IAEA Symposium On Thermodynamics of Nuclear Materials* (IAEA, Vienna, 1962).
[46] M. D. Silver, P. A. Farrar, and K. L. Komarek, Trans. Metall. Soc. AIME **227**, 876 (1963).
[47] G. E. Murch and R. J. Thorn, Acta Metall. **27**, 201 (1979).
[48] M. S. Blanter and L. B. Magalas, Scr. Mater. **43**, 435 (2000).